The Purported Square Ice in Bilayer Graphene is a Nanoscale, Monolayer Object

Tod A. Pascal, Craig P. Schwartz, Keith V. Lawler, and David Prendergast

Supplementary Materials

1. Computational Methods:

Density Functional Theory Calculations: Plane-wave, periodic DFT calculations were carried out using the Vienna Ab initio Software Package (VASP) [1, 2]. The projector-augmented wave (PAW) method [3, 4] was used to describe the electron-ion interactions and the generalized-gradient approximation with the vdW-DF2-type non-local correlation functional [5] was used to treat the long-range dispersion interactions. The plane-wave basis set is truncated at 400 eV and the first Brillouin zone is sampled with a 5 × 5 × 1 uniform Monkhorst-Pack grid of k-points to ensure the electronic charge density was converged. The potential energy binding curves of an isolated water on graphene were investigated on a flat two-dimensional extended 5x5 supercell. The distance between the oxygen atom and the graphene plane was varied from 2.0 to 6.0 Å in 0.1Å increments for four different orientations of the water molecules.

Carbon – Water Forcefield Fitting Procedure: We fit the four QM binding curves (Boltzmann weighted to ensure an accurate description of the relative binding energy minima) of an isolated water molecule on graphene to Buckingham potentials while simultaneously optimizing the carbon PQEq parameters (see below). Our optimization employed a least-squares fit using the Newton-Raphson minimization scheme. The optimized parameters are given in Table S1 and the comparisons to the QM energies are given in Table S2. Further details will be provided in a forthcoming manuscript.

Description of Computational Systems: Extensive MD simulations were initiated from water molecules randomly dispersed within a 40x40 nm^2 graphene bilayer, created from a 92x83x2 replication of the orthorhombic graphene cell (8 atom supercell with a = 4.275Å, b = 4.9367Å, c = 11.0Å, $\alpha=\beta=\gamma=90^o$). Systems with 200, 300, 400, 500, 600, 800, 1000, 1200, 1400, 1600, 1800, 2000, 2225, 2500, 2750, 3000, 3250, 3500, 3750, 4500, 5500 and 6500 water molecules were considered.

Equilibrium Molecular Dynamics Simulations: The charge on each atom was evaluated every time step (0.5 fs) as the overlap of Slater-type *ns*-orbitals within the QEq scheme of Rappe and Goddard[6]. We modified the LAMMPS code to allow for QEq calculations using *ns*-Slater type orbitals, according to an implementation in the GULP[7] 4.0 simulation engine. The OH bonds and HOH angle of the water molecules were constrained each time step using the RATTLE algorithm [8], with a convergence tolerance of 10^{-5}. The long range electrostatic interactions were obtained using the PPPM method [9] with a tolerance of 10^{-6}. The van der

Waals interactions were calculated using a 10Å cutoff, employing a cubic spline from 9Å to ensure consistent energies and forces.

Accelerated Molecular Dynamics Simulations: Initial systems were equilibrated using our standard procedure[10], where after initial energy minimization at 0K, we equilibrated the x and y components of the stress tensor by means of 10ns simulation in the constant temperature, constant pressure (NPT) ensemble. This was followed by 50ns of canonical (NVT) MD simulations. Finally, once equilibrated, the system was subjected to at least 100ns of nonequilibrium meta-dynamics[11, 12] simulations, sampling the Q_2,Q_5 subspace through an external biasing potential, formed by the addition of a 0.01 eV Gaussian function (0.01Å width) every 10ps. The version of the COLVARS module[13] implemented in LAMMPS was extended to allow for the collective variables employing the Steinhardt[14] Q_2 and Q_5 bond order parameters, according to an implementation in the DL_POLY Classic code[15, 16], and used to apply the metadynamics scheme. When determining the Q value of each oxygen atom, we considered neighboring oxygens within a 3.2Å cutoff. Convergence typically occurred after 50ns after which the collective variables were diffusive.

Enthalpy and Entropy Calculations: Candidate structures were identified by inspection and their positions and velocities used as input to 500ps constant temperature, constant volume (NVT) MD simulations. For all N, both the SqI and EWD structures were structurally stable on this timescale. Snapshots of the system (atomic velocities and coordinates) were saved every 2fs in 50ps windows (a total of 10 individual trajectories). For each trajectory, quantum corrected entropy and enthalpy were obtained from post-trajectory analysis using a code that implements the Two-Phase Thermodynamics (2PT) method [17-20]. The reported values were the statistical mean and standard deviations of the 10 trajectories.

Simulated Core-level Spectra: All EELS/XANES simulations were made using constrained orbital-occupancy DFT[21, 22] within the XCH formalism, detailed elsewhere [23]. The core excited oxygen atom was represented with a pseudopotential generated with a $1s^1\ 2s^2\ 2p^5$ configuration. All calculations utilized Vanderbilt ultrasoft pseudopotentials[24] to describe the core−valence electron interactions. All spectra were calculated using PBE with QuantumESPRESSO [25]. Spectral calculations were aligned based on an experimental reference spectrum (gas phase O_2) in a previous work [26] and a theoretical alignment scheme [27]. Calculated spectra were numerically broadened with a Gaussian convolution of either 2.5 eV (EELS) or 0.5 eV (XANES) FWHM unless noted otherwise.

2. Square ice unit cell

a = b = 5.64Å, c = 20.00Å, α=β=γ=90.00°

atom	fract_x	fract_y	fract_z
O	0.250000	0.250000	0.500000
H	0.423982	0.238297	0.499713
H	0.238295	0.423984	0.500179
O	0.250000	0.750000	0.500000
H	0.261701	0.923982	0.500253
H	0.076020	0.738297	0.499697
O	0.750000	0.250000	0.500000
H	0.738299	0.076016	0.500176
H	0.923973	0.261703	0.499447
O	0.750000	0.750000	0.500000
H	0.576023	0.761705	0.500462
H	0.761705	0.576016	0.500071

3. EWD Blister Dimension Analysis

According to Boddeti and coworkers[28], as first derived by Hencky[29] and later corrected by Williams[30] and Wan and Mai[31], we can relate vertical blister height δ and the blister radius a to the internal pressure p

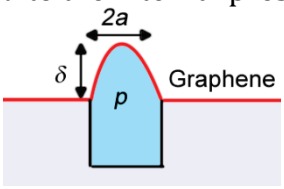

according to

$$\delta = C_2 \left(\frac{pa^4}{Et} \right)^{\frac{1}{3}} \quad (1)$$

We were interested in seeing if this macroscopic continuum model was valid for nanoscale EWD droplets. Table S3 lists the x,y,z dimensions of EWD droplets with various amounts of water molecules N:

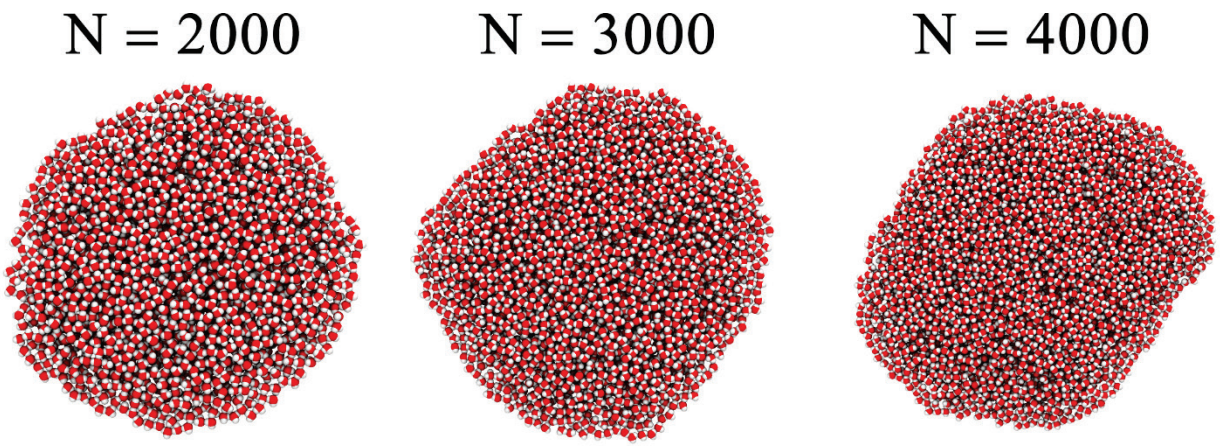

as well as the internal volume (V). From our equilibrium MD simulations of these droplets, we calculated the internal water stress (σ) and determined the internal pressure from the trace of the stress tensor, i.e.

$P = -(1/3V)[\sigma_{xx} + \sigma_{yy} + \sigma_{xx}]$ (2)

We take $a = (l_x + l_y)/4 + \chi$ and $\delta = l_z/2 + \chi$, where $\chi = 2.1$Å is the carbon–water van der Waals exclusion, obtained from the density plot of water next to the irregular EWD interface:

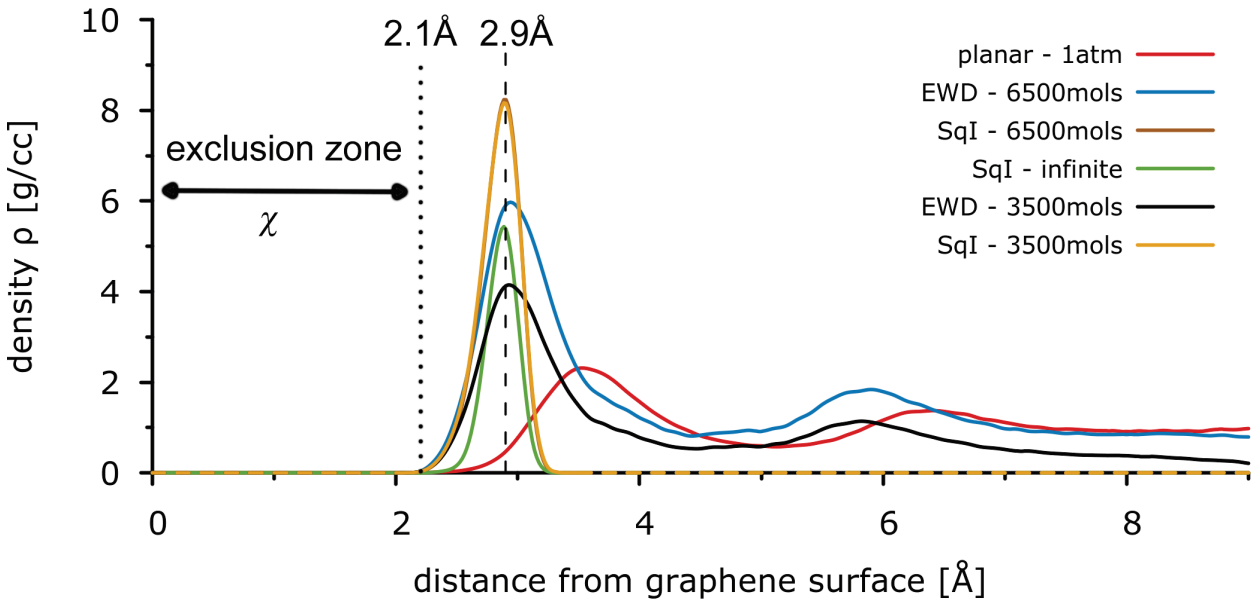

The above density plot includes data for various sized EWD droplets and SqI flakes, as well as the planar graphene water interface at 1atm pressure. The vertical dashed line is at position of the 1st peak maximum at 2.9Å for Ewd and SqI (3.65Å for the planar interface). The vertical dotted line denotes χ.

According to equation (1), if the Hencky model holds, a plot of δ^3 *vs* pa^4 is a straight line with slope $2C_2^3/Et$ (the factor of 2 accounts for the presence of a double blister here):

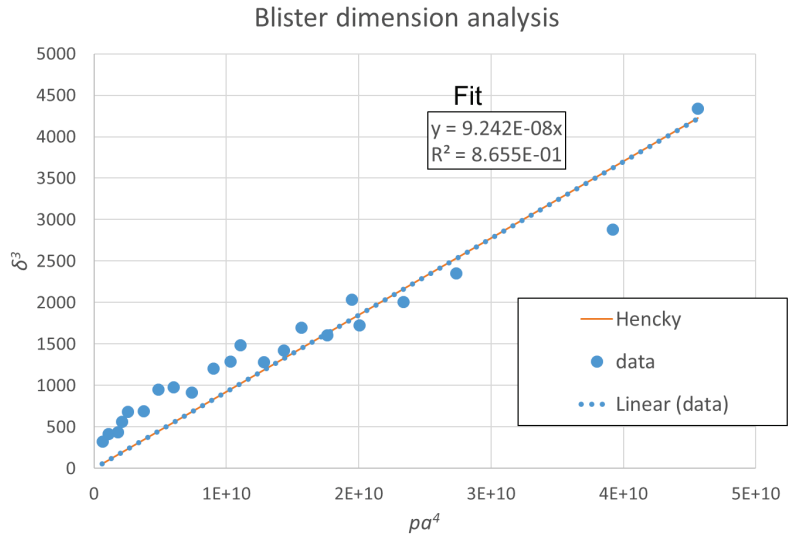

The constant C_2 = 0.687 used by Boddeti is determined numerically based on the in-plane Poisson ratio and Young's modulus of graphene, μ_{21}= 0.16 and Et = 340 N/m, respectively. It succeeds in describing graphene blisters at much larger sizes (100's of nm). Yet, we find the size and shape of the EWD water droplets closely follows this same relation (for sizes < 6000 water molecules, i.e., where the EWD is roughly circular in the plane). Therefore, we can trust that the resulting large (GPa) pressures are realistic.

4. Tables

Table S1: Nonbonding forcefield parameters used in this study. The water-water interactions are described using the TIP4P/Fq forcefield [32] while the carbon-carbon interactions are described using the QMFF-Cx forcefield [33]. The water-graphene interactions are obtained by fitting high level binding energy curves of an isolated water molecule on an infinite sheet to Buckingham potentials and carbon QEq [6] parameters (denoted the MF[3] forcefield). The H-O and H-H vdW interactions are zero as suggested by the TIP4P/Fq forcefield.

Parameter	Interaction type	Parameter Type	Value
O-C	[a]Buck vdW	A (eV)	583.95
		C (eV)	18.42
		ρ	0.31
H-C	Buck vdW	A	39.25
		C	5.74×10^{-4}
		ρ	0.38
O-O	[b]LJ vdW	ε_0 (eV)	0.01242
		r_0 (A)	3.159
C	QEq[c]	χ (eV)	5.14
		γ (eV)	5.90
		ζ (1/Å)	1.57
O	QEq	χ	2.97
		γ	16.11
		ζ	1.63
H	QEq[c]	χ	0.00
		γ	15.30
		ζ	0.90

[a]van der Waals interactions through the Buckingham potential: $E = Ae^{-r/\rho} - \frac{C}{r^6}$

[b] vdW interactions through the Lennard Jones 12-6 potential: $E = \varepsilon_0 \left[\left(\frac{r_0}{r} \right)^{12} - 2 \left(\frac{r_0}{r} \right)^{6} \right]$

[c]Charges obtained through the charge equilibration formalism of Rappe and Goddard[6]

Table S2: Comparison of the binding energies (eV) of an isolated water molecule centered on a graphene sheet from DFT calculations, the MF[3] and the Werder et al. [34] forcefields. The energy minimum distance (Å) is given in parenthesis. Four water geometries were considered: flat (dipole moment parallel to the plane), o-down (dipole moment anti-perpendicular to the plane), 2h-down (dipole moment perpendicular to the plane) and 1h-down (OH vector perpendicular to the plane)

water Orientation	DFT[a]	MF[3]	Werder
Flat	-0.105 (3.2)	-0.118 (3.3)	-0.047 (2.8)
o-down	-0.112 (3.2)	-0.122 (3.2)	-0.047 (2.8)
1h-down	-0.122 (3.4)	-0.157 (3.7)	-0.047 (2.8)
2h-down	-0.118 (3.4)	-0.1402 (3.6)	-0.047 (2.8)

Table S3: Geometrical parameters (Å), surface area (Å^2) and internal volume V (Å^3) and internal pressure p (GPa) of water encapsulated in bilayer graphene for the EWD and SqI phases. The surface area (s.a.) of the EWD phase was obtained from the MSMS code[35]. The pressure p = -Tr(σ)/3V, where σ is the 3x3 water stress tensor.

N	EWD						SqI					
	lx	**ly**	**lz**	**s.a.**	**V**	***p***	**lx**	**ly**	**lz**	**s.a.**	**V**	***p***
200	38.7	38.1	9.5	2687	4014	3.03	45.7	44.7	6.9	3346	3730	2.25
300	46.1	44.5	10.8	3727	6155	2.93	49.4	55.9	7.0	4966	5633	2.14
400	51.5	52.4	11.0	4700	8349	2.85	60.7	64.5	6.7	6530	7525	2.12
500	55.4	54.3	12.3	5302	10717	2.74	72.4	70.4	6.7	8166	9429	2.06
600	57.4	59.3	13.5	6044	13028	2.68	79.0	75.0	7.0	9811	11335	2.11
800	64.5	65.9	13.5	7468	17681	2.58	88.2	91.7	6.9	13014	15119	2.06
1000	70.0	71.0	15.5	8735	22440	2.48	100.4	100.9	6.7	16172	18964	2.02
1200	75.0	75.6	15.7	9881	27238	2.40	118.4	103.3	7.1	19346	22793	2.03
1400	79.6	80.7	15.2	11045	32060	2.33	122.1	113.9	6.7	22622	26646	2.05
1600	84.4	85.8	17.1	12109	36888	2.27	139.4	116.3	6.8	25743	30425	2.01
1800	88.8	88.9	17.6	13128	41808	2.20	129.5	137.4	7.0	29011	34284	2.02
2000	91.1	91.7	18.6	14394	47178	2.12	137.3	144.5	6.7	32483	38295	2.00
2250	95.3	96.4	17.5	15619	53420	2.05	149.2	153.6	6.6	36464	43065	2.01
2500	98.5	100.2	18.3	16353	59228	1.99	151.8	164.6	7.1	40361	47844	2.02
2750	102.2	102.9	19.7	17464	65511	1.93	174.2	168.6	6.8	44394	52783	2.00
3000	107.0	106.4	19.2	18475	71860	1.86	169.4	182.0	6.9	48238	57205	2.02
3250	108.1	112.7	21.2	19577	78155	1.80	159.4	208.7	6.9	49759	62935	1.99
3500	110.6	113.8	19.8	20383	84583	1.74	202.8	198.7	6.7	54512	67712	1.99
3750	118.6	117.4	21.0	22280	91514	1.68	186.2	224.1	6.6	60673	72077	1.99
4500	120.9	131.2	22.4	24821	110898	1.52	212.7	211.0	6.9	72563	86391	2.01
5500	142.1	143.8	24.3	28309	137169	1.34	243.5	234.5	7.0	88508	105534	2.00
6500	153.8	153.6	28.4	30838	164106	1.17	248.0	254.5	7.1	104708	124841	2.00

Table S4: Fitting constants (kJ/mol; J/mol/K for entropy) and constituent components for the thermodynamics model obtained from MD simulations at 298K. See figures E6-E10 for plots of the various components.

	component	Value
graphene	C–C binding	$\alpha_1 x^2+\beta_1 x$, $\alpha_1 = 0.0002$ $\beta_1 = 7.17$
	strain	$\alpha_2 x^2+\beta_2 x$ $\alpha_2 = 0.0001$ $\beta_2 = -0.71$
water–graphene binding		$\alpha_3 x^2+\beta_3 x$ $\alpha_3 = -0.0002$ $\beta_3 = -4.73$
Water	enthalpy	$\beta_4 = -4.54$
	entropy	$\chi x^2+\delta x$ $\chi = -0.0016$ $\delta = -4.61$

$\alpha = \alpha_1 + \alpha_2 + \alpha_3 = 0.0001; \beta = \beta_1 + \beta_2 + \beta_3 + \beta_4 = -2.81$

Table S5: Comparison of the difference in thermodynamics (meV/H_2O) between the SqI and EWD water phases (1600 water molecules) in bilayer graphene for various water forcefields. In all cases, we describe the water – graphene interactions using the O-C and H-C parameters in Table 1. The free energy barrier ΔG* for transitioning from the EWD to SqI phases during our accelerated MD simulations is also presented.

Water model	ΔG(EWD-SqI)	ΔH	TΔS	ΔG*
TIP4P-Fq	-19±3	-370±3	-350±5	+567±30
TIP4P/2005	-32±3	-118±2	-86±10	+412±55
TIP4P/2005f	-12±7	-250±5	-238±18	+370±72
SPC/Ew	-15±3	-75±7	-60±12	+350±50
TIP3P	-28±6	-121±8	-93±13	+231±25
F3C	-5±4	-152±3	-147±12	+124±30

5. Figures

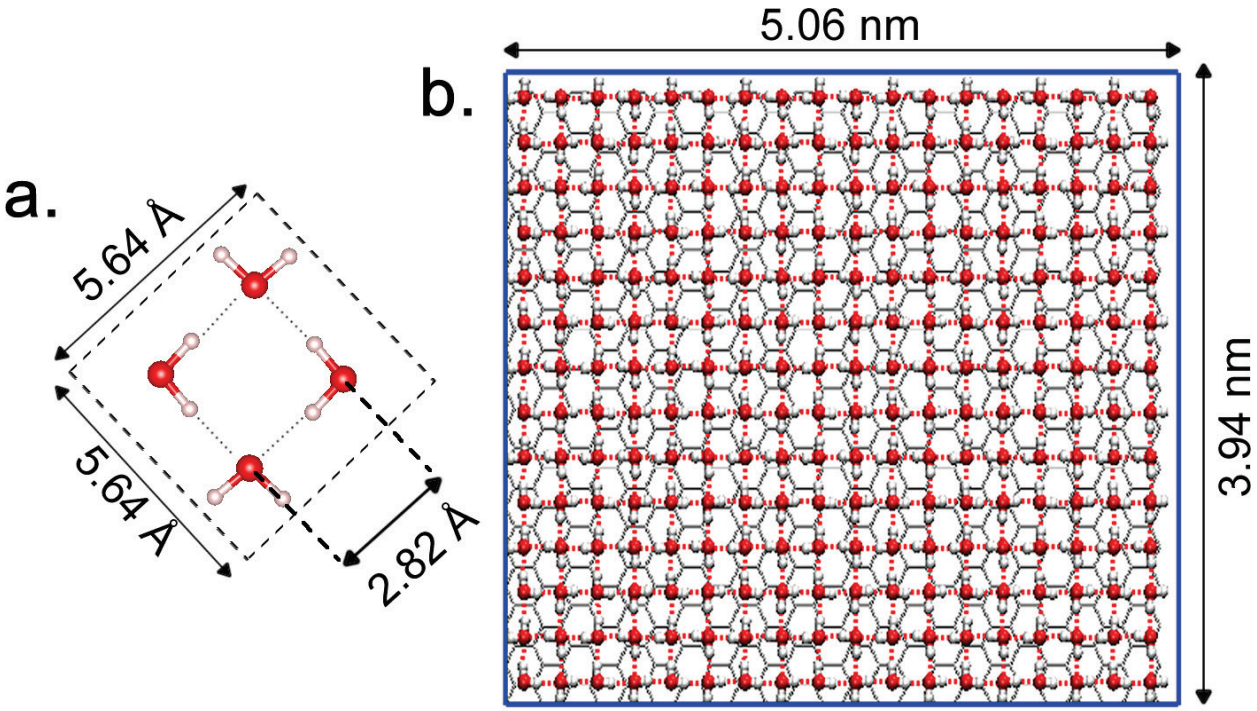

Figure S1 | a. Schematic of four water square ice unit cell. The 2.82Å oxygen-oxygen distance is show. The atomic coordinates are provided in supplementary materials. **b.** Square ice in graphene unit cell, comprising a 9x7 super cell of **a.** with a 12x8 supercell of orthorhombic bilayer graphene.

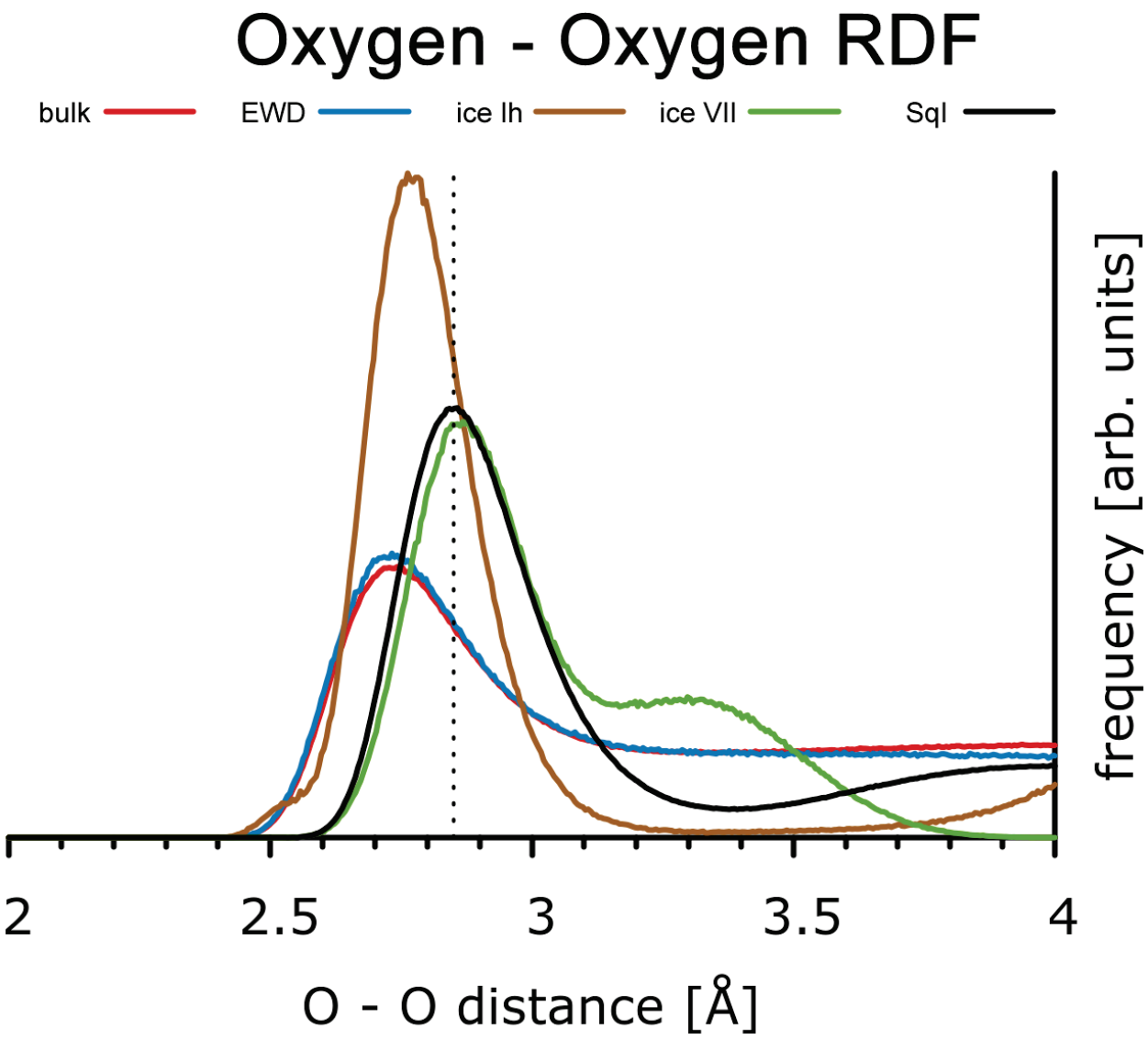

Figure S2 | Normalized oxygen-oxygen radial distribution functions. Values from 50ns equilibrium MD simulations in the bulk liquid phase (red line: T = 298K, P = 1bar), hexagonal ice Ih (brown line: T = 220K, P = 1bar), ice VII (green line: T = 298K, P = 30,000 bar) and a 4500 molecule EWD (blue line) and SqI (black line) phases of water encapsulated in a 40x40 nm^2 bilayer graphene are shown. The experimentally observed O-O distance of square ice (2.83 Å) is shown in dashed black line as a reference.

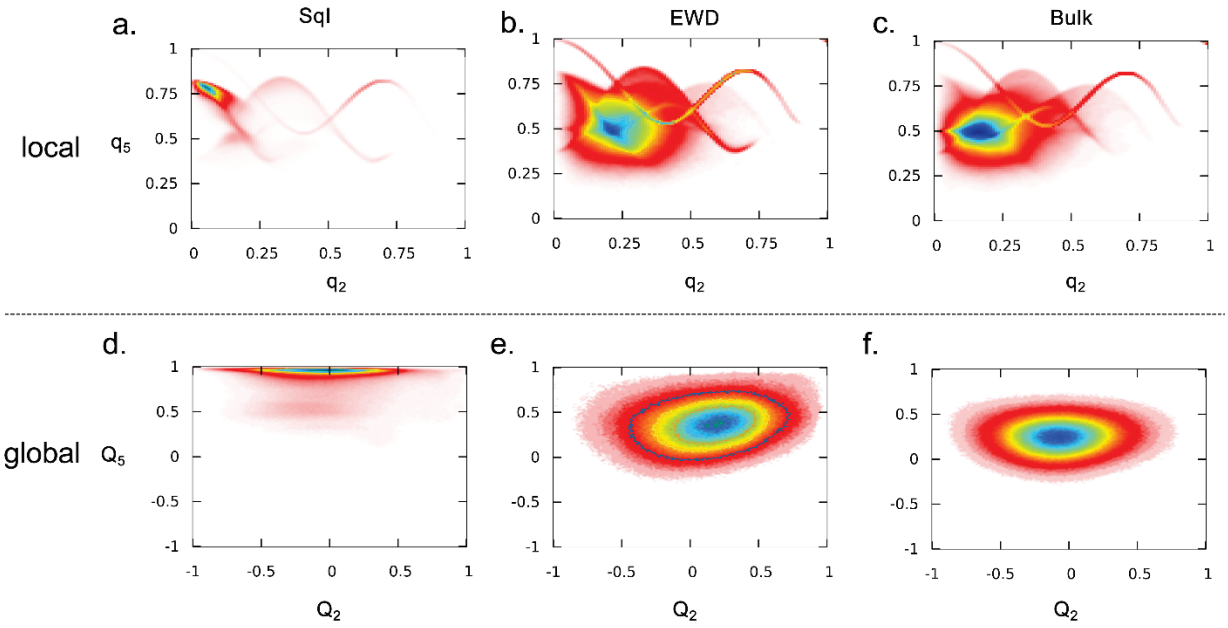

Figure S3 | 2D population analysis of the Steinhardt bond order parameters[14] (BOP). Values are obtained from 10ns equilibrium MD simulations of the indicated thermodynamic state for a 1600 water molecule system. FES corresponding to the **a.** SqI **b.** EWD and **c.** bulk water phases, as probed by the local parameters (q_2,q_5). The local parameters are defined as the norm of the complex BOP vector, are always positive, and therefore differ from the more popular global parameters (Q_2,Q_5) (**d**-**f**) which are defined as the real part of the complex dot product of the BOP vector with each neighbor[36]. In either method of analysis, SqI occupies a unique, non-overlapping region of phase space compared to EWD. Specifically, square ice occupies a region in the 2D thermodynamic phase space defined by $-0.25<Q_2<0.25$ and $0.95<Q_5<1.00$, while EWD occupies $-0.50<Q_2<0.50$ and $0.00<Q_5<0.50$.

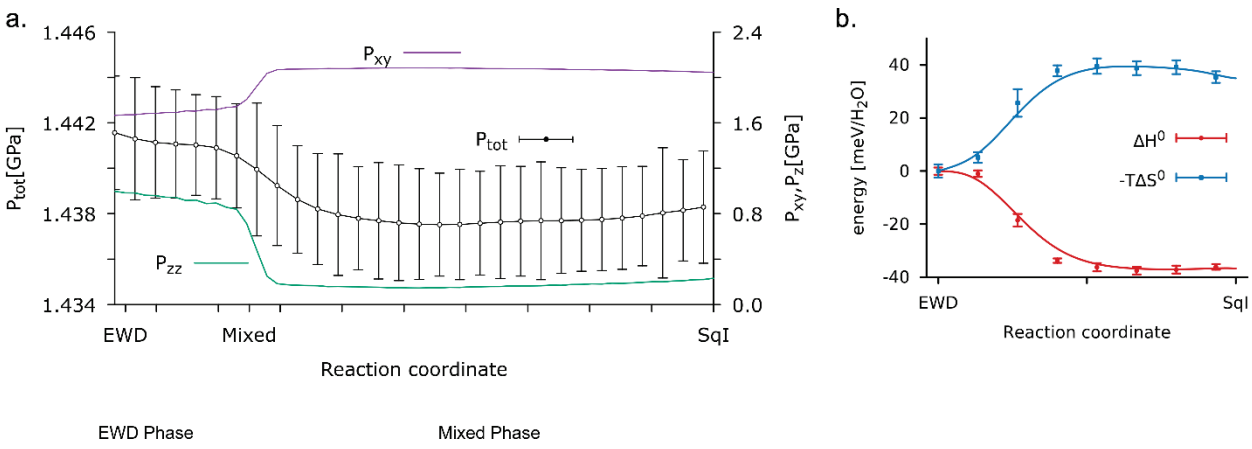

Figure S4 | Thermodynamics of bilayer graphene encapsulated water (N=1600). a. Change in the total internal water pressure (P_{tot} - black line) along the minimum free-energy path (MFP). The standard deviation is indicated. We separately plot the in-plane (P_{xy} = $[P_{xx}+P_{yy}]/2$ - purple line) and out of plane (P_{zz} - teal line) pressure on the right y-axis. All pressure are in GPa. **b.** Profile of relative SqI entropy ($-T\Delta S$ - blue circles) and enthalpy (ΔH - red squares) along the MFP. The data (symbols) are shown with a smooth cubic spline function (lines) for presentation purposes. The uncertainty is indicated by error bars.

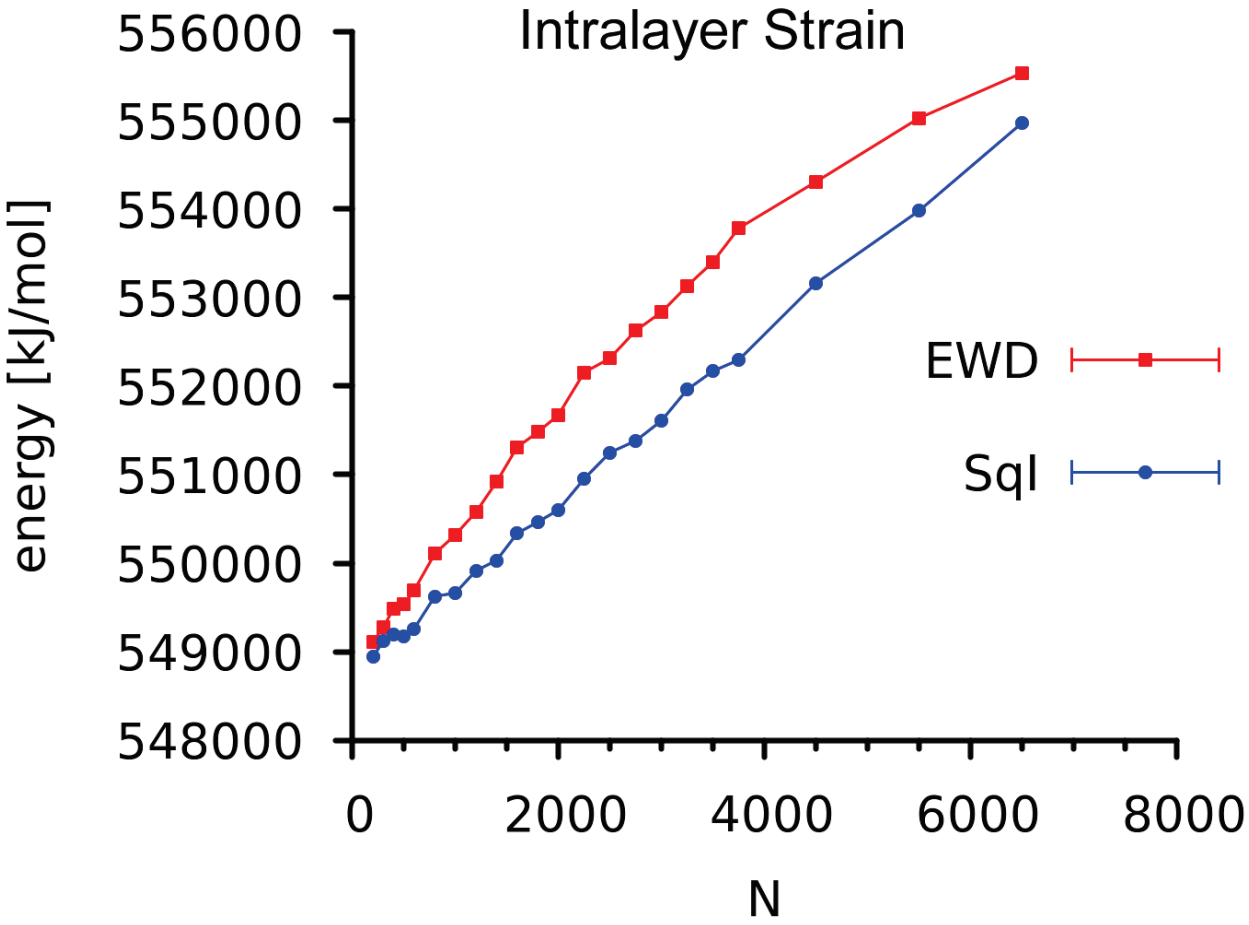

Figure S5 | Interlayer strain energy of graphene. Data for EWD (red squares) and SqI (blue circles) phase as shown as a function of number of water molecules (N)

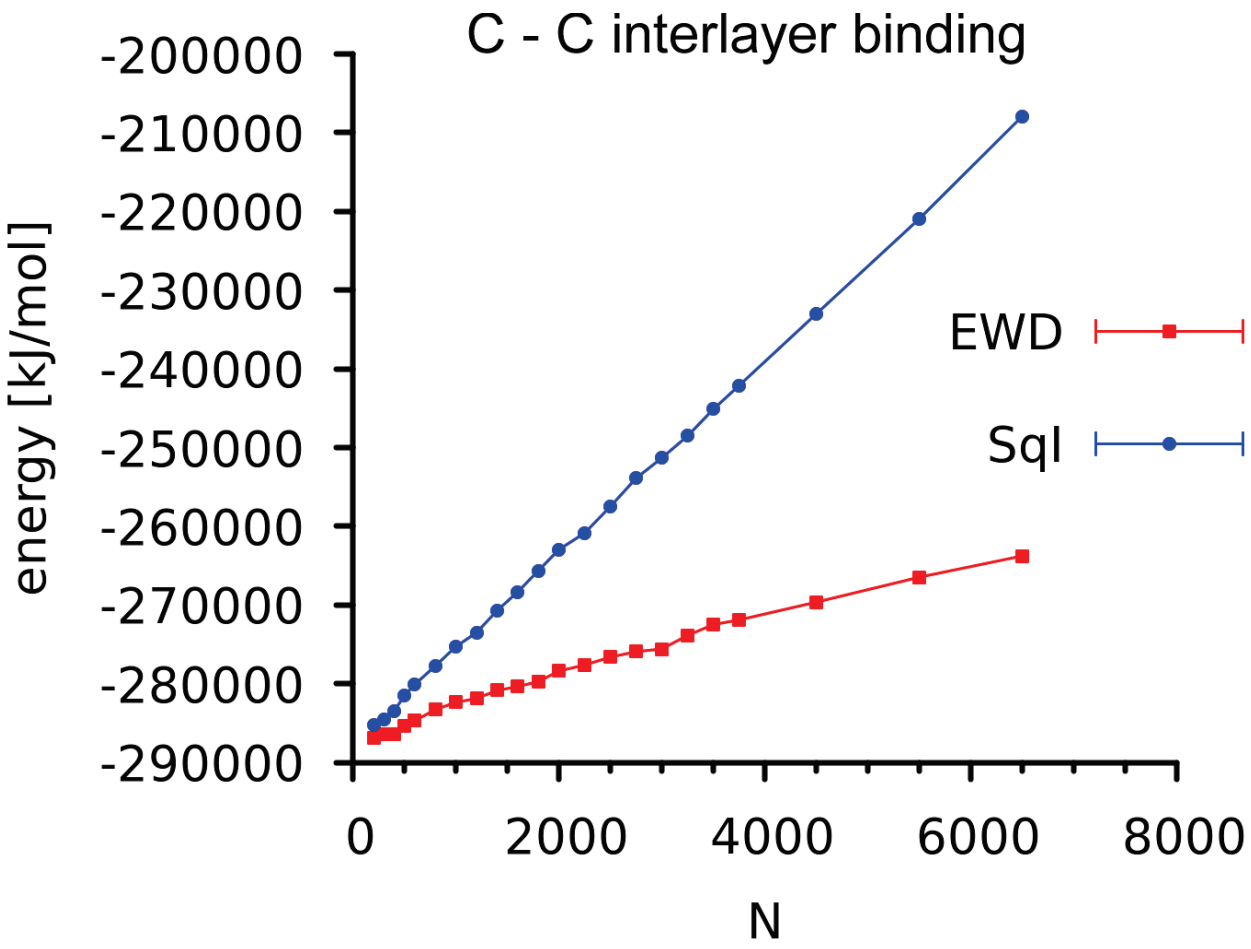

Figure S6 | Plot of the graphene–graphene interlayer binding energy as a function of number of water molecules (N) for the EWD (red squares) and SqI (blue circles) phase from MD simulations. The calculated values (points) are connected with lines to guide the eyes.

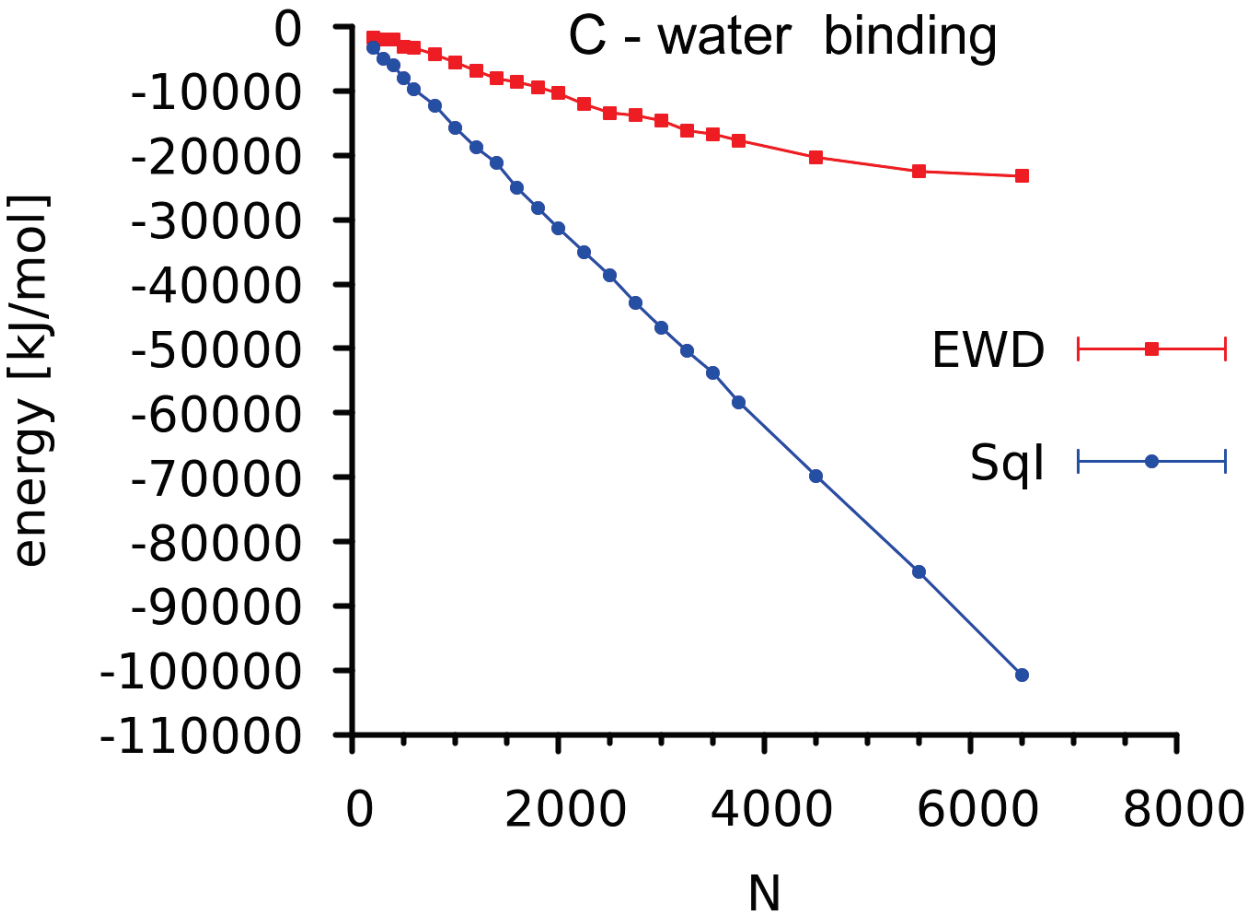

Figure S7 | Water–Graphene Binding. Plot of the water–graphene interaction energy as a function of number of water molecules (N) for the EWD (red squares) and SqI (blue circles) phase from MD simulations.

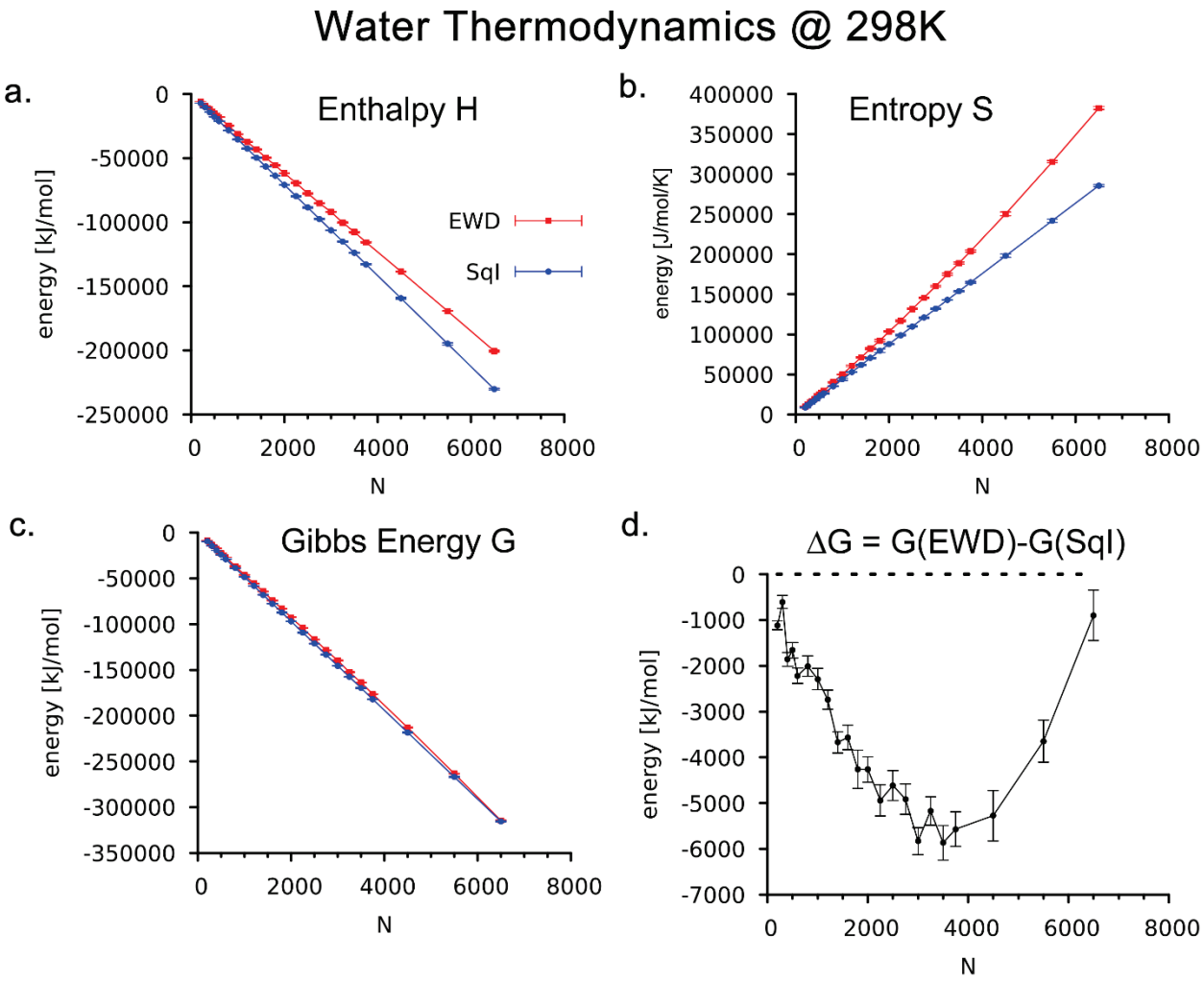

Figure S8 | Thermodynamics of Water molecules encapsulated in bilayer graphene. **a.** Absolute Enthalpy of water molecules encapsulated in bilayer graphene as a function of number of molecules (N) for the EWD (red squares) and SqI (blue circles) phase from MD simulations. **b.** Entropy of water molecules in bilayer graphene **c.** Gibbs "free" energy of water molecules in bilayer graphene **d.** Relative Gibbs energy ΔG

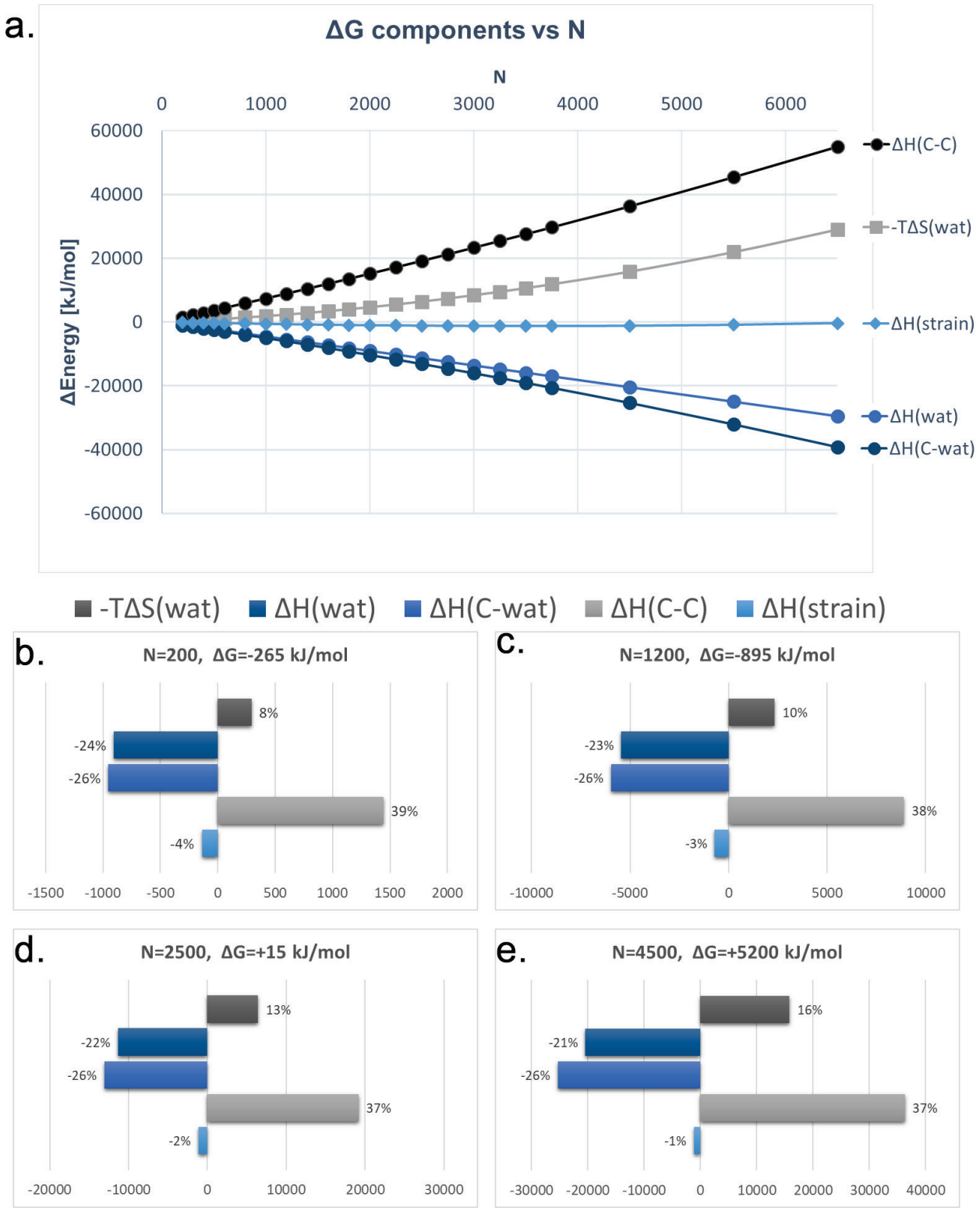

Figure S9 | SqI-EWD stability. a. Plot of the components of ΔG(SqI-EWD) as a function of size (N) obtained from model Hamiltonian in Eq 1. The five terms of Eqn 1 are plotted as indicated. **b-e.** Percent contribution of each term to the overall free energy for N = 200, 1200, 2500 and 4500 respectively (as indicated in the chart title).

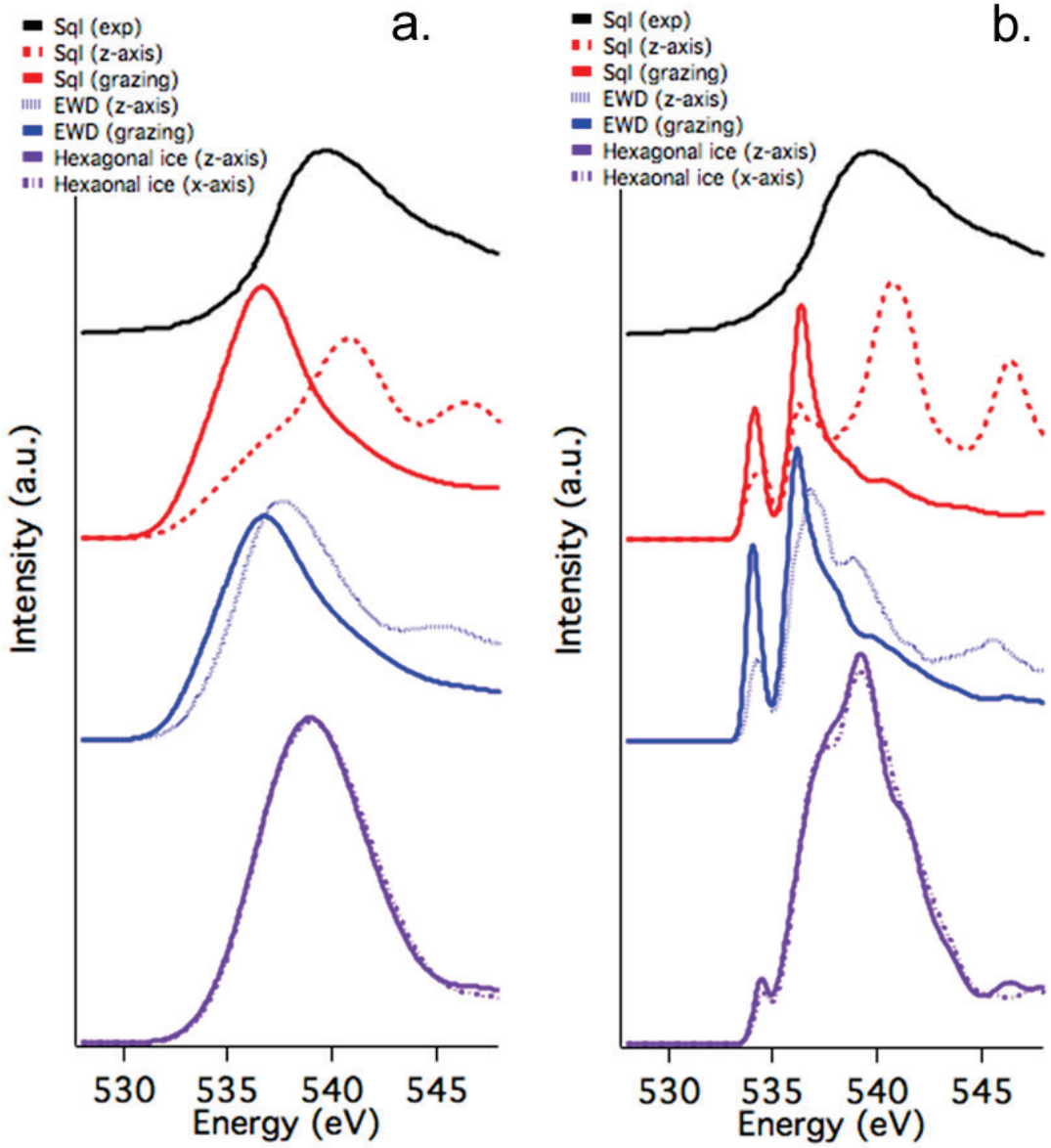

Figure S10 | EELS spectrum of water and ice. a. Comparison of EELS spectra of the experimental square ice[37] (black) to the simulated spectra of SqI (red) along the z-axis (dashed) and at grazing incidence (solid), EWD (blue) at z-axis (solid) and grazing incidence (dashed) and hexagonal ice along two different axes (purple solid and dashed). All simulated spectra are broadened by convoluting to a 2.5 eV Gaussian function, which is similar to the experimental EELS resolution at this energy. The calculated ice spectra agree well with the literature, although we note that the literature EELS hexagonal ice spectrum[38, 39] is misaligned as compared to several x-ray Raman studies. **b.** Same as **a.** but with only 0.5 eV broadening, which might more closely resemble an X-ray absorption study.

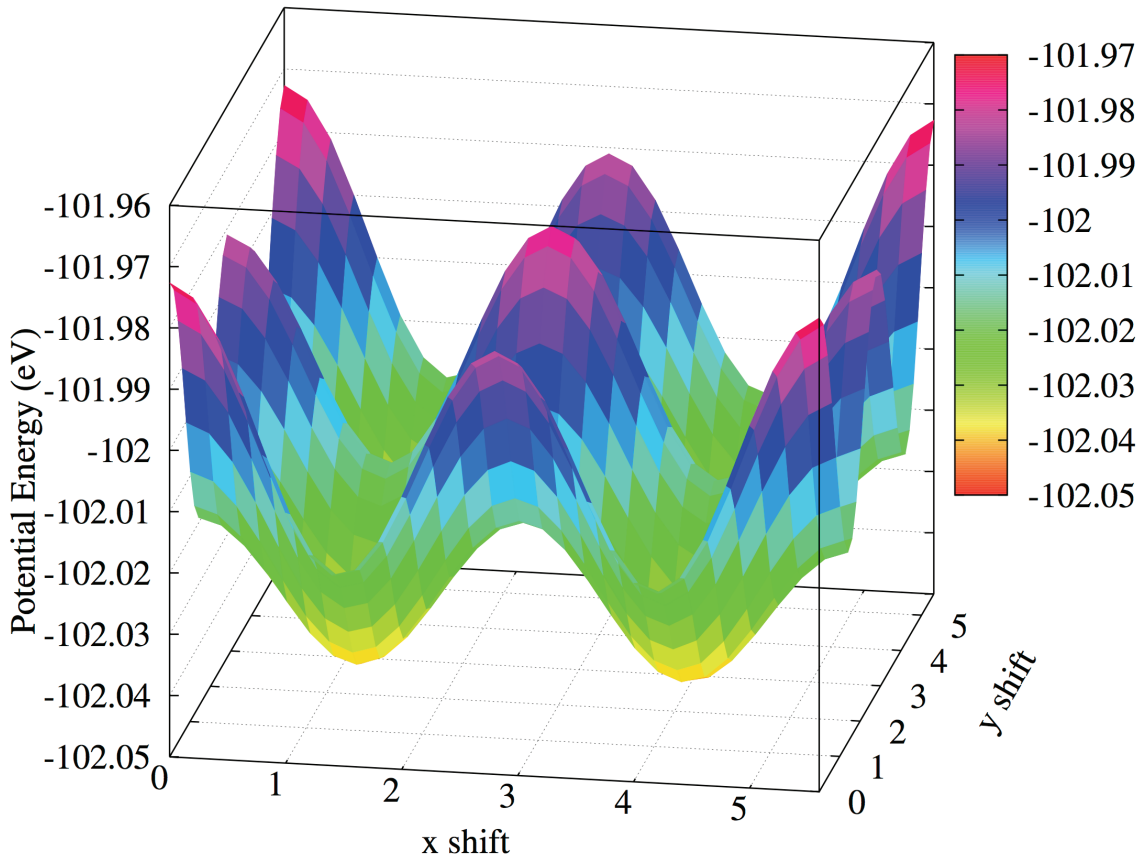

Figure S11 | Water layer–layer potential energy surface, constructed by sliding the four molecule square ice unit cell (figure S1a) on another static layer separated by 3.5Å. The most favorable stacking configuration is with an x-shift of 1.4Å and a y-shift of 1.4Å, corresponding to AB stacking. The AA stacked configuration is unfavorable by 8.593 meV/water.

Reference

[1] G. Kresse, and J. Furthmuller, Comput. Mater. Sci. **6** (1996) 15.
[2] G. Kresse, and J. Hafner, Phys. Rev. B **47** (1993) 558.
[3] P. E. Blochl, Phys. Rev. B **50** (1994) 17953.
[4] G. Kresse, and D. Joubert, Physical Review B **59** (1999) 1758.
[5] K. Lee *et al.*, Phys. Rev. B **82** (2010) 081101.
[6] A. K. Rappe, and W. A. Goddard, J. Phys. Chem. **95** (1991) 3358.
[7] J. D. Gale, and A. L. Rohl, Molecular Simulation **29** (2003) 291.
[8] H. C. Andersen, J. Comput. Phys. **52** (1983) 24.
[9] R. W. Hockney, and J. W. Eastwood, *Computer Simulation Using Particles* (Taylor & Francis, New York, 1989),
[10] T. A. Pascal, S. T. Lin, and W. A. Goddard, 3rd, Physical chemistry chemical physics : PCCP **13** (2011) 169.
[11] A. Laio, and F. L. Gervasio, Reports on Progress in Physics **71** (2008) 126601.
[12] G. Bussi, A. Laio, and M. Parrinello, Phys. Rev. Lett. **96** (2006) 090601.
[13] G. Fiorin, M. L. Klein, and J. Hénin, Mol Phys **111** (2013) 3345.
[14] P. J. Steinhardt, D. R. Nelson, and M. Ronchetti, Phys. Rev. B **28** (1983) 784.
[15] W. Smith, T. Forester, and I. Todorov, 2010).
[16] W. Smith, C. Yong, and P. Rodger, Molecular Simulation **28** (2002) 385.
[17] T. A. Pascal, S. T. Lin, and W. A. Goddard, Physical Chemistry Chemical Physics **13** (2011) 169.
[18] S.-T. Lin, P. K. Maiti, and W. A. Goddard, J. Phys. Chem. B **114** (2010) 8191.
[19] S. T. Lin, M. Blanco, and W. A. Goddard, J. Chem. Phys. **119** (2003) 11792.
[20] T. A. Pascal, and W. A. Goddard, J. Phys. Chem. B **118** (2014) 5943.
[21] P. Hohenberg, and W. Kohn, Phys. Rev. **136** (1964) B864.
[22] W. Kohn, and L. J. Sham, Phys. Rev. **140** (1965) A1133.
[23] D. Prendergast, and G. Galli, Phys. Rev. Lett. **96** (2006) 215502.
[24] G. Kresse, and D. Joubert, Phys. Rev. B **59** (1999) 1758.
[25] P. Giannozzi *et al.*, J. Phys.: Condens. Matter **21** (2009) 395502.
[26] P. Jiang *et al.*, J. Chem. Phys. **138** (2013) 024704.
[27] A. H. England *et al.*, Chemical Physics Letters **514** (2011) 187.
[28] N. G. Boddeti *et al.*, Journal of Applied Mechanics **80** (2013) 040909.
[29] H. Hencky, Zeitschrift fur Mathematik und Physik **63** (1915) 311.
[30] J. Williams, International Journal of Fracture **87** (1997) 265.
[31] K.-T. Wan, and Y.-W. Mai, Acta metallurgica et materialia **43** (1995) 4109.
[32] S. W. Rick, S. J. Stuart, and B. J. Berne, J. Chem. Phys. **101** (1994) 6141.
[33] T. A. Pascal, N. Karasawa, and W. A. Goddard, J. Chem. Phys. **133**, 134114 (2010)
[34] T. Werder *et al.*, J. Phys. Chem. B **107** (2003) 1345.
[35] M. F. Sanner, A. J. Olson, and J. C. Spehner, Biopolymers **38** (1996) 305.
[36] P. R. ten Wolde, M. J. Ruiz-Montero, and D. Frenkel, J. Chem. Phys. **104** (1996) 9932.
[37] G. Algara-Siller *et al.*, Nature **519** (2015) 443.
[38] K. Kobayashi, M. Koshino, and K. Suenaga, Phys. Rev. Lett. **106** (2011) 206101.
[39] T. Pylkkanen *et al.*, J. Phys. Chem. B **114** (2010) 3804.